

RESEARCH LETTER

10.1002/2016GL071568

Key Points:

- Demonstrates flux transfer events are not necessarily force free
- Finds that in non-force-free FTEs, the magnetic force is balanced by the ion pressure gradient force; the electron pressure can be ignored
- Minimum variance analysis on the magnetic pressure gradient force gives the best estimate of the axial direction of flux ropes

Correspondence to:

C. Zhao,
 czhao@igpp.ucla.edu

Citation:

Zhao, C., et al. (2016), Force balance at the magnetopause determined with MMS: Application to flux transfer events, *Geophys. Res. Lett.*, 43, 11,941–11,947, doi:10.1002/2016GL071568.

Received 12 OCT 2016

Accepted 16 NOV 2016

Accepted article online 18 NOV 2016

Published online 9 DEC 2016

Force balance at the magnetopause determined with MMS: Application to flux transfer events

C. Zhao¹ , C. T. Russell¹ , R. J. Strangeway¹ , S. M. Petrinec² , W. R. Paterson³ , M. Zhou⁴, B. J. Anderson⁵ , W. Baumjohann⁶ , K. R. Bromund³ , M. Chutter⁷ , D. Fischer⁶ , G. Le³ , R. Nakamura⁶ , F. Plaschke⁶ , J. A. Slavin⁸ , R. B. Torbert⁷ , and H. Y. Wei¹

¹Department of Earth, Planetary and Space Sciences, University of California, Los Angeles, California, USA, ²Lockheed Martin ATC, Palo Alto, California, USA, ³NASA Goddard Space Flight Center, Greenbelt, Maryland, USA, ⁴Department of Physics and Astronomy, University of California, Los Angeles, California, USA, ⁵Applied Physics Laboratory, The Johns Hopkins University, Laurel, Maryland, USA, ⁶Space Research Institute, Austrian Academy of Sciences, Graz, Austria, ⁷Department of Physics, University of New Hampshire, Durham, New Hampshire, USA, ⁸Department of Climate, Space Sciences and Engineering, University of Michigan, Ann Arbor, Michigan, USA

Abstract The Magnetospheric Multiscale mission (MMS) consists of four identical spacecraft forming a closely separated (≤ 10 km) and nearly regular tetrahedron. This configuration enables the decoupling of spatial and temporal variations and allows the calculation of the spatial gradients of plasma and electromagnetic field quantities. We make full use of the well cross-calibrated MMS magnetometers and fast plasma instruments measurements to calculate both the magnetic and plasma forces in flux transfer events (FTEs) and evaluate the relative contributions of different forces to the magnetopause momentum variation. This analysis demonstrates that some but not all FTEs, consistent with previous studies, are indeed force-free structures in which the magnetic pressure force balances the magnetic curvature force. Furthermore, we contrast these events with FTE events that have non-force-free signatures.

1. Introduction

Flux transfer events (FTEs) couple solar wind mass, momentum, and energy to the magnetosphere through their magnetic connection between the magnetosheath plasma and the magnetospheric plasma. They are characterized by a unipolar magnetic field enhancement along the axial direction of the structure and a transient bipolar magnetic field signature in the direction normal to the structure [Russell and Elphic, 1978]. There are also some FTEs with a decrease of magnetic field strength in the center, additional to the typical unipolar magnetic field magnitude structure. This type of FTE is referred to as a crater FTE [Labelle et al., 1987; Farrugia et al., 1988]. The physical interpretation of the observed FTE phenomena is still subject to debate. The prevailing model of FTE structures is that of a magnetic flux rope [Elphic, 1990]. Other concepts for explaining these structures, like magnetopause waves [Sibeck, 1990], have proven to be inconsistent with the observations. Many attempts have been made to fit the observational FTE data to a parameterized flux rope model. Some of them are based on the Lundquist [1950] force-free with circular cross-section flux rope model by, e.g., Hasegawa et al. [2007], Scholer [1995], and Zhang et al. [2008]. Others use the assumption that the flux rope is not magnetically force free but still in force balance with the magnetic field and plasma pressures [Elphic and Russell, 1983; Farrugia et al., 2016]. The four MMS spacecraft with their close separation and intercalibrated plasma and field instruments allow these hypotheses to be tested.

The NASA Magnetospheric Multiscale (MMS) Mission consists of four identical spacecraft, which form a nearly regular tetrahedron [Burch et al., 2016]. The separation of the spacecraft can be as close as 10 km at the apogee during Phase 1a of the prime mission, with a separation knowledge of 10 m. The magnetic field, electric field, and plasma instruments on board each spacecraft are identical and cross calibrated. In the region of interest (greater than 9 Earth radii (R_E) away from the Earth) the Fast Plasma Instruments (FPI) on board the satellites operates at an unprecedented rapid cadence. In burst mode, the temporal resolution is a sample every 150 ms for ions and 30 ms for electrons, which is comparable to but longer than the 7.8 ms burst-mode magnetic field data. These features facilitate the joint analysis of plasma and fields measurements to definitively and quantitatively answer physical questions related to the magnetic reconnection process by examining the variations of the directly measured physical quantities.

In this paper, we first briefly describe the data and methodology used to perform the pressure and curvature forces calculation. We then analyze four separate FTE events and present evidence that there are different types of FTEs.

2. Data and Methodology

The data used in this paper are the magnetic field measurements from the fluxgate magnetometer [Russell *et al.*, 2016] and the plasma measurements from the Fast Plasma Instrument (FPI) [Pollock *et al.*, 2016], which are on board each of the four Magnetospheric Multiscale (MMS) spacecraft [Burch *et al.*, 2016]. The data are collected at slightly different times from the instruments on the four spacecraft, so all data are interpolated to the time stamp of the magnetic field measurement of MMS1 for the cross-spacecraft and cross-instrument calculations. The times associated with the magnetometer measurements are also assigned to the center of each sample interval. However, the time stamp of the telemetered FPI data is associated with the beginning of each sample interval. In order to work on a common time descriptor between instrument data sets, we therefore assign a time to the FPI data that is shifted by half of its sample period. Thus, the two data products are consistent with each other and are centered on the same time.

The physical foundation of our discussion is based on the magnetohydrodynamic momentum equation, given by equation (1), while equations (2) and (3) give the parallel and perpendicular components of equation (1).

Elphic *et al.* [1980] suggested that some flux ropes are force-free structures with current only along the field direction, such that both of the two terms $\mathbf{j} \times \mathbf{B}$ and $\nabla \cdot \mathbf{P}$ in the right-hand side of equation (1) are equal to zero.

$$\rho \frac{D\mathbf{u}}{Dt} = \mathbf{j} \times \mathbf{B} - \nabla \cdot \mathbf{P} \quad (1)$$

$$\rho \frac{D\mathbf{u}}{Dt} \Big|_{\parallel} = -\mathbf{b} (\mathbf{b} \cdot \nabla P_{\parallel}) + \frac{(P_{\parallel} - P_{\perp})}{2P_m} (\mathbf{b} \cdot \nabla P_m) \mathbf{b} \quad (2)$$

$$\rho \frac{D\mathbf{u}}{Dt} \Big|_{\perp} = (-\nabla_{\perp} P_m) + (-\nabla_{\perp} P_{i\perp}) + (-\nabla_{\perp} P_{e\perp}) + (2P_m + (P_{i\perp} - P_{i\parallel}) + (P_{e\perp} - P_{e\parallel})) \kappa_c \quad (3)$$

where $P_m = \frac{B^2}{2\mu_0}$ is the magnetic pressure and $\kappa_c = (\mathbf{b} \cdot \nabla) \mathbf{b}$ is the curvature of the magnetic field.

The terms on the right-hand side of equation (3) are the perpendicular gradient of magnetic pressure, the perpendicular gradient of ion perpendicular pressure, the perpendicular gradient of electron perpendicular pressure, the magnetic curvature force associated with the magnetic pressure and the magnetic curvature force associated with the ion and electron anisotropy, respectively.

The numerical method related to the calculation of the different terms in equation (3) is the calculation of the gradient of a vector or scalar field [Harvey, 1998]. Assume $\mathbf{k} = \nabla m$ is the gradient tensor of the scalar field m . Define the function S to be the summation of the residue of the first-order Taylor expansion of m :

$$S = \sum_{\alpha=1}^N \sum_{\beta=1}^N |[\mathbf{k} \cdot (\mathbf{r}_{\alpha} - \mathbf{r}_{\beta}) - (m_{\alpha} - m_{\beta})]|^2 \quad (4)$$

\mathbf{r}_{α} in equation (4) is the location of spacecraft α in mesocenter frame, where the mesocenter is defined as the average location of the four spacecraft.

In order to obtain the best estimation of $\mathbf{k} = \nabla m$, we need $\frac{\delta S}{\delta k_{ij}} = 0$. By solving this equation, we obtain

$$k_j = \frac{1}{N^2} [\sum_{\alpha \neq \beta} (m_{\alpha} - m_{\beta}) (r_{\alpha k} - r_{\beta k})] R_{kj}^{-1} \quad (5)$$

where $R_{kj} = \frac{1}{N} \sum_{\alpha=1}^N r_{\alpha i} r_{\alpha j}$.

Similarly, the gradient \mathbf{k} of a vector \mathbf{b} is

$$k_{ij} = \frac{1}{N^2} [\sum_{\alpha \neq \beta} (b_{\alpha i} - b_{\beta i}) (r_{\alpha k} - r_{\beta k})] R_{kj}^{-1}. \quad (6)$$

For each flux transfer event, the physical quantities are examined in the local FTE-LMN coordinates as illustrated schematically in Figure 1. Because both the current and the magnetic field component along the

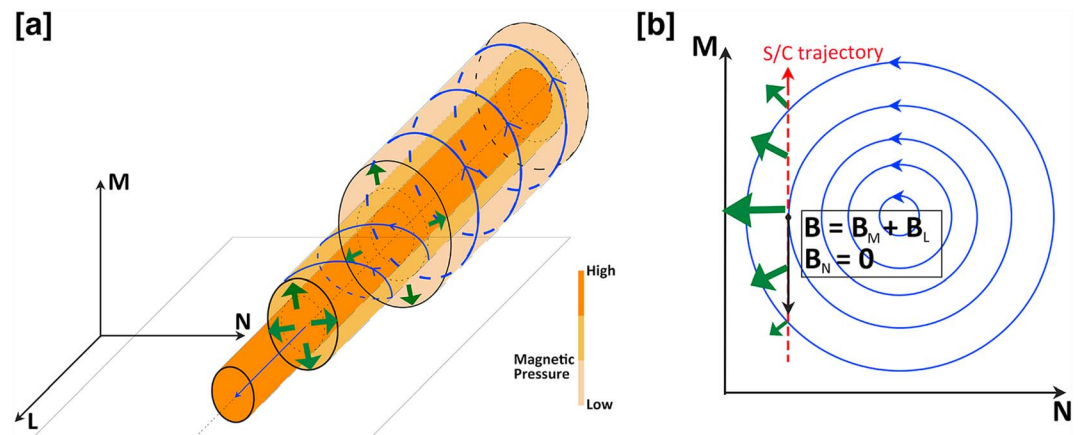


Figure 1. Schematic picture of (a) the flux rope 3-D structure and (b) the cross-section perpendicular to the axis of the flux rope. The blue arrows show the magnetic field line, green arrows point along the pressure gradient direction, while the red arrow is the spacecraft trajectory. Dark, medium, and light yellow fill color illustrate the different pressure values.

direction of rope axis are not constant, the minimum variance analysis on them would not result in an accurate rope axial direction. However, based on the assumption that the flux rope pressure profile is uniform along the axial direction, the pressure gradient acts only perpendicular to the rope axis (green vectors in Figure 1). Thus, minimum variance analysis on the magnetic pressure gradient will lead to an accurate rope axial direction; thereby, we define this direction as L direction. When the spacecraft is at its closest encounter to the FTE, i.e., when the magnetic field magnitude maximizes in the time series, the field can only have two components (as shown in Figure 1b), one along the rope axis and the other along the spacecraft trajectory projected in the M - N plane, which means $\mathbf{B}_{\max} = \mathbf{B}_M + \mathbf{B}_L$. So the N direction can be obtained through $\mathbf{N} = (\mathbf{B}_{\max} \times \mathbf{L}) / |\mathbf{B}_{\max} \times \mathbf{L}|$. Last, \mathbf{M} completes the right-hand coordinate system.

3. Force Free and Non-Force-Free Flux Transfer Event Cases

Figure 2a shows an overview of the first event on 16 October 2015. This appears to be a partial magnetopause crossing. The MMS fleet went from the magnetosphere into the magnetopause boundary layer at around 13:04:15 UT and went back into the magnetosphere at around 13:04:52 UT, and there is no evidence of pure magnetosheath properties recorded by the MMS fleet. Two flux transfer events (FTEs), or flux ropes, are found in the middle of this partial magnetopause crossing. They have been interpreted to be two adjacent islands formed by magnetic reconnection [Eastwood *et al.*, 2016]. Figure 2b is an overview of another FTE event on 14 December 2015. The MMS spacecraft left the magnetopause at around 00:58:00 UT and went partially through the magnetopause and back into the magnetosphere at around 00:59:40 UT. The flux rope is embedded in the magnetopause layer and encountered the MMS fleet from 00:58:57 UT to 00:59:01 UT. The last row in Figures 2a and 2b contains the current calculated from the curlometer. It is clearly demonstrated that the current in the magnetopause is flowing in both the parallel and perpendicular directions with comparable strengths, while the current inside the FTEs mainly flows along the magnetic field line. The expansion in Figures 3a–3c shows the detailed structure of these three FTEs in the local FTE-LMN coordinates. In each plot in Figure 3, lines a and d denote the start and end of each FTE event, respectively, while line b denotes the time of maximum magnetic field strength inside the FTE.

In Figures 3a–3c, the magnetic field profiles exhibit bipolar structure in the N component and a unipolar structure in the L component, which is strong evidence for encountering a flux transfer event [Russell and Elphic, 1979]. The second event is nearly symmetric with respect to line b_2 , the time when the magnetic field magnitude reaches its maximum. The third event, on the other hand, is asymmetric around the maximum of $|\mathbf{B}|$. The first event exhibits the signature of a crater FTE. This topological difference in magnetic profile is evidence that an asymmetry could exist in the FTE, i.e., it may not be a perfectly circular flux rope. Using the multispacecraft timing method, the velocity and direction (in LMN coordinates) of the three events are measured to be 260 km/s [0.44, -0.86, 0.27], 260 km/s [0.70, -0.67, -0.22], and 180 km/s [0.70 -0.71, 0.08], respectively. The cross-section diameter of the three FTEs are 950 km, 1050 km, and 900 km, respectively.

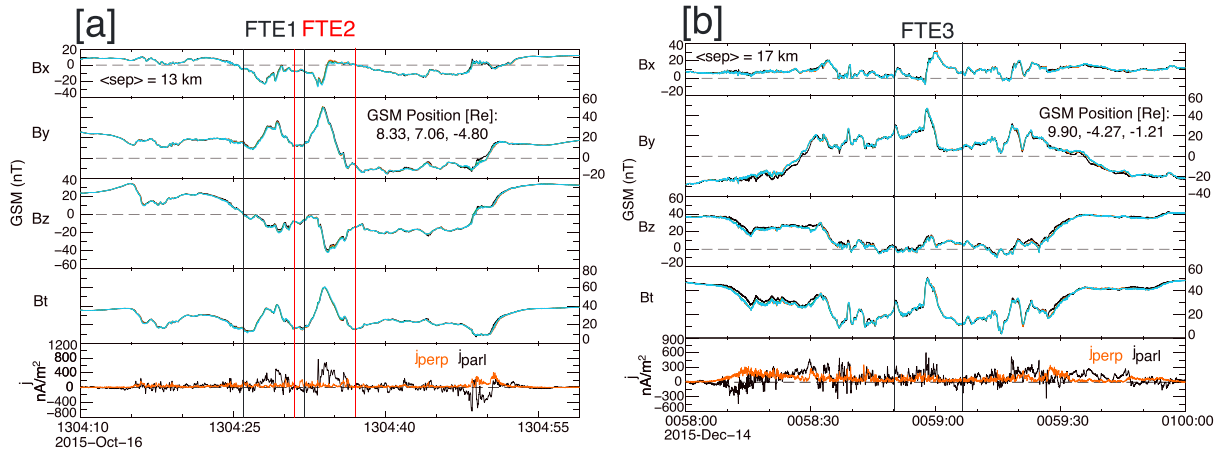


Figure 2. Overview of three flux transfer event embedded between two partial magnetopause crossing, (a) the magnetopause crossing on 16 October 2015 and two FTEs; (b) the magnetopause crossing on 14 December 2015 and one FTE contained within it. For both plots, the first four panels are the GSM X, Y, Z components, and intensity of the magnetic field of the four MMS spacecraft in black (MMS1), orange (MMS2), light green (MMS3), and light blue (MMS4), respectively. The fifth row shows the current from the curlometer, the black trace is the current parallel to the magnetic field, and the orange trace is the perpendicular current.

The sixth row of each event shows the parallel and perpendicular current from the curlometer calculation. The parallel component dominates the current flowing through the flux transfer event in all three cases with a magnitude of about 500 nA/m^2 . The current drops to around zero in the middle of the three FTEs (marked by lines c_1 , c_2 , and c_3 , respectively), but surprisingly not coincident with the maximum of magnetic field strength. The perpendicular current is nearly an order of magnitude smaller than the parallel current throughout FTE1 and FTE2, which reveals the near force-free property of the flux transfer events, while the magnitude of the perpendicular current is comparable to the parallel current in part of FTE3 (between line d3 and e3). However, there is no absolute threshold of current strength to determine whether the structure is magnetic force free or not. A plausible way to classify force-free and non-force-free structures would be to determine

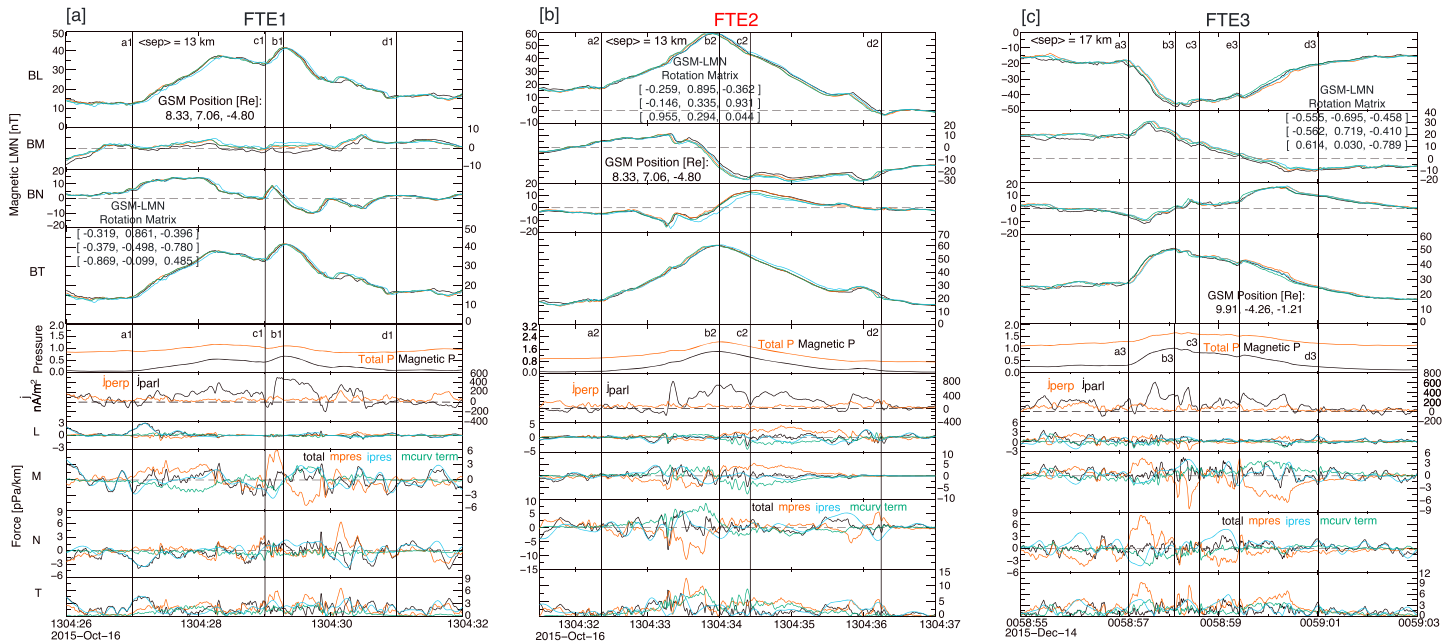


Figure 3. Three FTEs, the first four rows are the L , M , N component, and intensity of the magnetic field for the four MMS spacecraft in black (MMS1), orange (MMS2), light green (MMS3), and light blue (MMS4), respectively. The fifth row is the magnetic pressure in orange and total pressure in black. The sixth row is the current from the curlometer, the black trace is the current parallel to the magnetic field, and the orange trace is the perpendicular current. The last four rows are the L , M , N direction, and total of the force analysis, with the black being the summation of different force contribution, the orange being the magnetic pressure gradient force, the light blue being ion pressure gradient force, and light green being the magnetic curvature force.

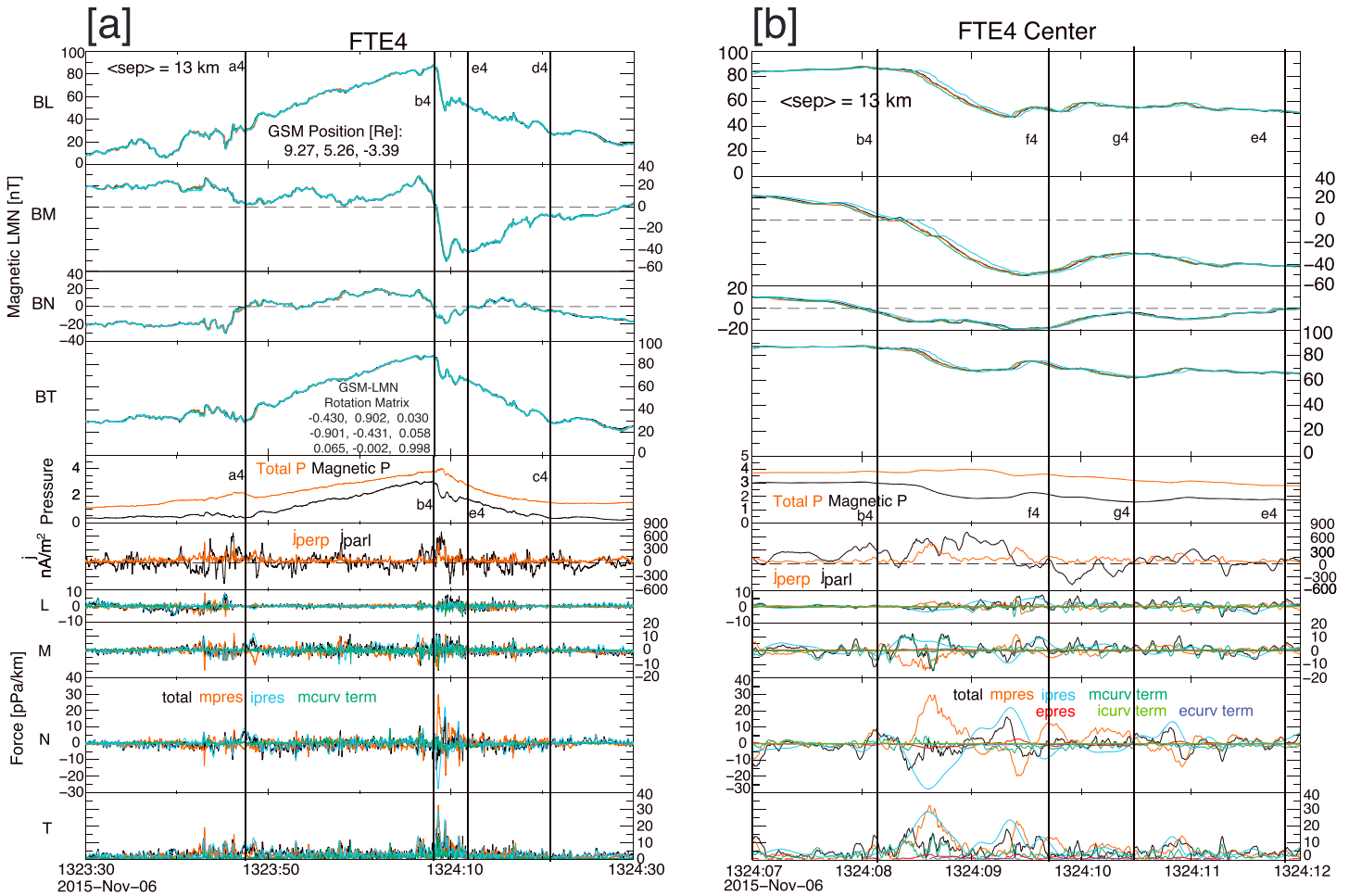


Figure 4. (a) The fourth FTE, which is non-force free and (b) the center part of this FTE, where large magnetic and plasma force exist. The plot format is similar to Figure 3, despite that three curves are added into the last four panels of Figure 4b. They are the electron pressure gradient in red, curvature force associated with ion pressure anisotropy in light green and curvature force associated with electron anisotropy in dark blue.

the relative dominant terms in the momentum equation to check whether or not they are purely magnetic terms. A FTE where purely magnetic terms determine the momentum balance would be a force-free structure.

This property is examined in more detail in the remaining panels in Figure 3. The last four panels of each displayed event are the three components as well as the magnitude of the magnetic pressure force components (in orange), the magnetic curvature force (in dark green) component of the $\mathbf{j} \times \mathbf{B}$ force, the ion pressure gradient (in light blue), and the total force exerted on the FTEs (in black). These force analyses definitively show that the magnetic curvature force in FTE1 and FTE2 is always opposite the magnetic pressure force and results in much smaller total magnetic force (i.e., $\mathbf{j} \times \mathbf{B}$ force). But the magnetic pressure and curvature force magnitudes vary considerably in these three events. The force magnitudes are 2 pPa/km and 8 pPa/km, respectively. In each individual event, the force profile also demonstrates apparent asymmetry. For example, in FTE2, the normal component of the force is much larger before the maximum of the magnetic field strength intensity than thereafter.

Although FTE3 shares a similar behavior to those of FTE1 and FTE2 (the magnetic curvature force opposes the magnetic pressure force), a significant difference is that the magnetic curvature force is much smaller than magnetic pressure force (especially in the normal direction) and results in a nonvanishing magnetic force in the case of FTE3. Also shown in the last two rows of Figure 3c, the nonzero $\mathbf{j} \times \mathbf{B}$ force is balanced by the ion pressure gradient force. So FTE3 is not a force-free structure but involves force balance between nonzero magnetic and plasma forces.

In order to prove that the non-force-free FTE3 is not unique, we present a fourth FTE (FTE4) in Figure 4a. The velocity of FTE4 is close to 146 km/s, which leads to a much larger diameter of 4700 km. The current in FTE4 is concentrated in the very central part of this FTE. The total magnetic force has two very large (~ 30 pPa/km) peaks in the center of this FTE. This force is also balanced by the ion pressure gradient force, similar to FTE3. In Figure 4b, for the 5 s interval (between b4 and e4 in Figure 4a) where the magnetic pressure force peaks is presented and shows evidence that the magnetic force is balanced by the ion pressure gradient force in the “crater” part of FTE3. In FTE4, the parallel current changes from along the magnetic field to antiparallel to the magnetic field marked by line f4 and g4, right after the ion pressure gradient and magnetic pressure gradients reach their maxima. This antiparallel current untwists the field line, providing evidence that the physical process inside the crater is very dynamic.

Also plotted in the last four rows of Figure 4b is the electron pressure gradient force (in dark red), the curvature force due to the ion anisotropy (in light green), and the curvature force due to the electron anisotropy (in dark blue). As shown in the figure, these three components of equation (3) are around zero, so they do not contribute significantly to the momentum variation of the FTEs compared to the ion pressure gradient force. This is expected because the temperature of electrons is usually much smaller than that of ions. This is also the case with the other three FTEs, although not explicitly shown in their force analysis plots.

4. Conclusions

The diagnostic capability of the MMS mission, with four identical satellites forming a closely separated tetrahedron with high-resolution plasma and magnetic field measurements, was fully exploited in this study to perform a quantitative analysis of the forces associated with the four flux transfer events. First, the force analysis procedure was used to determine the axial direction of the flux transfer event by estimating the minimum variation direction of the magnetic pressure force, because the flux rope does not push along its axis. The force analysis provides much more information than the current analysis by itself. Through this powerful tool enabled by the MMS mission, we demonstrate that there are force-free flux transfer event cases as predicted by Lundquist [1950] in which the magnetic pressure force is balanced by the magnetic curvature force. However, there are also FTEs in which the magnetic curvature force is not sufficient to balance the magnetic pressure force. Therefore, the plasma force and especially the ion pressure force must be taken into account in the FTE force balance, while the electron contribution is usually small and can be ignored. To study the dynamics of FTE, both the ion and magnetic structure must be examined.

Acknowledgments

This research was supported by the NASA Magnetospheric Multiscale Mission in association with NASA contract NNG04EB99C. The work at UCLA was supported through subcontract 06-001 with the University of New Hampshire. IRAP contributions to MMS FPI was supported by CNES and CNRS. We thank the entire MMS team and instrument leads for data access and support. The data presented in this paper are the L2 data of MMS and can be accessed from MMS Science Data Center (<https://lasp.colorado.edu/mms/sdc/public/>).

References

- Burch, J. L., et al. (2016), Electron-scale measurements of magnetic reconnection in space, *Science*, 352(6290), aaf2939, doi:10.1126/science.aaf2939.
- Eastwood, J. P., et al. (2016), Ion-scale secondary flux ropes generated by magnetopause reconnection as resolved by MMS, *Geophys. Res. Lett.*, 43, 4716–4724, doi:10.1002/2016gl068747.
- Elphic, R. C. (1990), *Observations of Flux Transfer Events: Are FTEs Flux Ropes, Islands, or Surface Waves?*, *Geophys. Monogr. Ser.*, pp. 455–471, AGU, Washington, D. C., doi:10.1029/GM058p0455.
- Elphic, R. C., and C. T. Russell (1983), Magnetic-flux ropes in the Venus ionosphere—Observations and models, *J. Geophys. Res.*, 88, 58–72, doi:10.1029/JA088iA01p00058.
- Elphic, R. C., C. T. Russell, J. A. Slavin, L. H. Brace, and A. F. Nagy (1980), The location of the dayside ionopause of Venus—Pioneer Venus Orbiter magnetometer observations, *Geophys. Res. Lett.*, 7, 561–564, doi:10.1029/GL007i008p00561.
- Farrugia, C. J., R. P. Rijnbeek, M. A. Saunders, D. J. Southwood, D. J. Rodgers, M. F. Smith, C. P. Chaloner, D. S. Hall, P. J. Christiansen, and L. J. C. Woolliscroft (1988), A multi-instrument study of flux transfer event structure, *J. Geophys. Res.*, 93, 14,465–14,477, doi:10.1029/JA093iA12p14465.
- Farrugia, C. J., et al. (2016), Magnetospheric Multiscale Mission observations and non-force free modeling of a flux transfer event immersed in a super-Alfvénic flow, *Geophys. Res. Lett.*, 43, 6070–6077, doi:10.1002/2016gl068758.
- Harvey, C. C. (1998), in *Spatial Gradients and the Volumetric Tensor, Analysis Methods for Multi-Spacecraft Data*, *ISSI Sci. Rep. Ser.*, vol. 1, edited by G. Paschmann and P. W. Daly, pp. 307–322, Observatoire de Paris-Meudon, Meudon, France.
- Hasegawa, H., R. Nakamura, M. Fujimoto, V. A. Sergeev, E. A. Lucek, H. Reme, and Y. Khotyaintsev (2007), Reconstruction of a bipolar magnetic signature in an earthward jet in the tail: Flux rope or 3D guide-field reconnection?, *J. Geophys. Res.*, 112, A11206, doi:10.1029/2007ja012492.
- Labelle, J., R. A. Treumann, G. Haerendel, O. H. Bauer, G. Paschmann, W. Baumjohann, H. Luhr, R. R. Anderson, H. C. Koons, and R. H. Holzworth (1987), AMPTE IRM observations of waves associated with flux-transfer events in the magnetosphere, *J. Geophys. Res.*, 92, 5827–5843, doi:10.1029/JA092iA06p05827.
- Lundquist, S. (1950), Magneto-Hydrostatic Fields, *Ark Fys.*, 2(4), 361–365.
- Pollock, C., et al. (2016), Fast plasma investigation for magnetospheric multiscale, *Space Sci. Rev.*, 199(1–4), 331–406, doi:10.1007/s11214-016-0245-4.
- Russell, C. T., and R. C. Elphic (1978), ISEE-1 and ISEE-2 observations of flux-transfer events on dayside magnetopause, *Eos Trans. AGU*, 59(12), 1162–1162.

- Russell, C. T., and R. C. Elphic (1979), ISEE observations of flux-transfer events at the dayside magnetopause, *Geophys. Res. Lett.*, *6*, 33–36, doi:10.1029/G1006i001p00033.
- Russell, C. T., et al. (2016), The magnetospheric multiscale magnetometers, *Space Sci. Rev.*, *199*(1–4), 189–256, doi:10.1007/s11214-014-0057-3.
- Scholer, M. (1995), Models of flux transfer events, in *Physics of the Magnetopause*, pp. 235–245, AGU, Washington, D. C., doi:10.1029/GM090p0235.
- Sibeck, D. G. (1990), A model for the transient magnetospheric response to sudden solar-wind dynamic pressure variations, *J. Geophys. Res.*, *95*, 3755–3771, doi:10.1029/JA095iA04p03755.
- Zhang, H., K. K. Khurana, M. G. Kivelson, V. Angelopoulos, Z. Y. Pu, Q. G. Zong, J. Liu, and X. Z. Zhou (2008), Modeling a force-free flux transfer event probed by multiple Time History of Events and Macroscale Interactions during Substorms (THEMIS) spacecraft, *J. Geophys. Res.*, *113*, A00C05, doi:10.1029/2008ja013451.